Received Date : 28-Aug-2015

Revised Date : 03-Mar-2016

Accepted Date : 04-Mar-2016

Article type : Research Report

Journal Section: Molecular & Synaptic Mechanisms

6-hydroxydopamine-induced Parkinson's disease-like degeneration generates acute micro- and astrogliosis in the nigrostriatal system but no Bioluminescence Imaging detectable alteration in adult neurogenesis

Inga B. Fricke[1,2], Thomas Viel[1,3], Maik M. Worlitzer[2], Franziska M. Collmann[1,4], Alexis Vrachimis[1,5], Andreas Faust[1], Lydia Wachsmuth[6], Cornelius Faber[6,10], Frédéric Dollé[7], Michael T. Kuhlmann[1], Klaus Schäfers[1,10], Sven Hermann[1], Jens C. Schwamborn[2,8], Andreas H. Jacobs[1,9,10].

1. European Institute for Molecular Imaging (EIMI), University of Münster, Münster, Germany.

2. ZMBE, Institute of Cell Biology, Stem Cell Biology and Regeneration Group, University of Münster, Münster, Germany.

3. Current address: PARCC, Inserm UMR 970, Université Paris Descartes, Paris, France.

4. Current address: In-vivo-NMR Laboratory, Max Planck Institute for Metabolism Research, Cologne, Germany.

5. Department of Nuclear Medicine, University Hospital Münster, Münster, Germany.

6. Department of Clinical Radiology, University Hospital Münster, Münster, Germany.

This article has been accepted for publication and undergone full peer review but has not been through the copyediting, typesetting, pagination and proofreading process, which may lead to differences between this version and the Version of Record. Please cite this article as doi: 10.1111/ejn.13232
This article is protected by copyright. All rights reserved.

7. CEA, I2BM, Service Hospitalier Frédéric Joliot, Orsay, France.

8. Luxembourg Centre for Systems Biomedicine (LCSB), University of Luxembourg, Esch-Belval, Luxembourg.

9. Department of Geriatric Medicine, Evangelische Kliniken, Johanniter Krankenhaus, Bonn, Germany.

10. DFG EXC 1003, Cluster of Excellence 'Cells in Motion', Münster, Germany.

Correspondence: Prof. Andreas H. Jacobs, MD
European Institute for Molecular Imaging (EIMI)
University of Münster
Waldeyerstr. 15
D-48149 Münster
Tel. +49 251 83 49300
Fax. +49 251 83 49313
ahjacobs@uni-muenster.de

Running title: Gliosis and neurogenesis post PD-like degeneration

Keywords: Parkinson's disease, 6-OHDA, neuroinflammation, [^{18}F]DPA-714, mouse

ABSTRACT

Parkinson's disease (PD) is a slowly progressing neurodegenerative disorder caused by loss of dopaminergic neurons in the substantia nigra (SN), leading to severe impairment in motor and non-motor functions. Endogenous subventricular zone (SVZ) neural stem cells constantly give birth to new cells which might serve as a possible source for regeneration in the adult brain. However, neurodegeneration is accompanied by neuroinflammation and dopamine depletion, potentially compromising regeneration. We therefore employed *in vivo* imaging

This article is protected by copyright. All rights reserved.

Accepted Article

methods to study striatal deafferentation ([^{123}I]Ioflupane SPECT, DaTscan^{TM}) and neuroinflammation in SN and striatum ([^{18}F]DPA-714 PET) in the intranigral 6-hydroxydopamine (6-OHDA) PD mouse model. Additionally, we transduced cells in the SVZ with a lentivirus encoding firefly luciferase and followed migration of progenitor cells in the SVZ – olfactory bulb (OB) axis via bioluminescence imaging (BLI) under disease and control conditions. We found that activation of microglia in the SN is an acute process coming along with the degeneration of dopaminergic cell bodies in the SN. Dopaminergic deafferentation of the striatum does not influence the generation of Dcx^{+} neuroblasts in the SVZ, but generates chronic astrogliosis in the nigrostriatal system.

1. INTRODUCTION

Parkinson's disease (PD) is characterised by loss of dopaminergic neurons in the substantia nigra (SN) and their striatal projections. PD is usually diagnosed after 50% of dopaminergic neurons in the SN and 80% of striatal dopamine are lost (Fearnley and Lees, 1991). As only symptomatic treatment is available, novel endogenous neuroregeneration approaches are desired.

The subventricular zone (SVZ) lining the lateral ventricles and the subgranular zone (SGZ) of the dentate gyrus generate progenitor cells that migrate to the olfactory bulb (OB) or granular cell layer. In the SVZ, slowly dividing radial glia-like cells give rise to transient amplifying cells, which themselves generate neuroblasts. Neuroblasts migrate long distances along the rostral migratory stream towards the OB, maturing and integrating into existing neural circuits (Ming and Song, 2011). Therefore, SVZ neuroblasts might serve as a source for new neurons in the diseased brain. However, endogenous neuroregeneration is insufficient or non-existent in PD, potentially due to disease-associated alterations in neurogenesis.

This article is protected by copyright. All rights reserved.

Accepted Article

Different studies report decreased (Baker et al., 2004, Höglinger et al., 2004), unchanged (van den Berge et al., 2011), or even increased (Aponso et al., 2008) progenitor cell proliferation after striatal dopamine depletion in PD patients and animal models. Moreover, dopaminergic neurodegeneration is accompanied by increased numbers of microglia in post-mortem PD-patients (Imamura et al., 2003, McGeer et al., 1988) as well as PD animal models (Czlonkowska et al., 1996). Depending on their plasticity, microglia can have favourable or detrimental effects on neurogenesis, and neuron survival (Bastos et al., 2008, Ekdahl et al., 2003, Sierra et al., 2010, Walton et al., 2006). Activated microglia, reactive astrocytes and infiltrating peripheral macrophages produce a variety of cytokines, chemokines, neurotransmitters, and reactive oxygen species, which affect the proportion of neuro- and gliogenesis, and the amount of progenitor cell proliferation.

Compared to conventional histological techniques, *in vivo* imaging reduces experimental animal numbers and allows for longitudinal studies. Single photon emission computed tomography (SPECT) using the tracer [^{123}I]Ioflupane, which has high binding affinity for the presynaptic dopamine transporters (DaT) (Booij et al., 1997a, Booij et al., 1997b), allows for detection of pathological changes in dopaminergic projections in patients and preclinical PD models. Translocator protein (TSPO) expression in healthy brain tissue is low (Giatzakis and Papadopoulos, 2004). High levels of TSPO expression in activated microglia and reactive astrocytes (Chen and Guilarte, 2008, Cosenza-Nashat et al., 2009, Lavisse et al., 2012, Scarf and Kassiou, 2011), allow for imaging of brain inflammation with positron emission tomography (PET) tracers targeting TSPO (Jacobs and Tavitian, 2012), such as [^{18}F]DPA-714 (Damont et al., 2013, Dollé et al., 2009, James et al., 2008). Bioluminescence imaging (BLI) was described as a tool to follow and quantify the migration of firefly luciferase transduced progenitor cells in the SVZ – OB axis *in vivo* (Reumers et al., 2008).

This article is protected by copyright. All rights reserved.

Accepted Article

Based on the hypothesis that dopaminergic neurodegeneration and the associated microglia activation affect subventricular neurogenesis, we aimed to monitor striatal deafferentation, neuroinflammation, and progenitor cell migration in a PD mouse model employing non-invasive multimodal imaging.

2. MATERIALS AND METHODS

2.1 Cell culture

Human HEK293T (kind gift of Dr. R. Thomas, Max Planck Institute for Metabolism Research, Cologne, Germany) and Gli36ΔEGFR (kind gift of Dr. David Louis, Molecular Neurooncology Laboratory, Massachusetts General Hospital, Boston, MA, USA) cells were grown as monolayer cultures in Dulbecco's modified Eagle's medium high glucose GlutaMAX (DMEM; Gibco, Darmstadt, Germany) supplemented with 10% foetal bovine serum (FBS; Invitrogen, Carlsbad, CA, USA) and 1x Penicillin/Streptomycin (P/S, Penicillin 1000 IU, Streptomycin 1000 µg/ml; PAA Laboratories, Cölbe, Germany) at 37°C and 5% CO_2/95% air.

2.2 Generation of reporter vectors

The pLKO.1-CMV-fLuc-IRES-mCherry plasmid (pLKO.1-CMV-LIC, Fig. S1) was constructed in two steps starting from the pLKO.1shControl+Luc plasmid created by G. Jungwirth (AG Jacobs, Max Planck Institute for Metabolism Research, Cologne, Germany) from the pLKO.1 vector (kind gift of Dr. R. Thomas, Max Planck Institute for Metabolism Research, Cologne, Germany). The first step consisted in introducing the mCherry gene from Kl13-pCDNA (created by Dr. K. Kruttwig, Max Planck Institute for Metabolism Research, Cologne, Germany). The sequence of the mCherry gene and the pLKO.1shControl+Luc plasmid were digested by NheI and EcoRI before ligation.

This article is protected by copyright. All rights reserved.

Accepted Article

Fluc-IRES was then amplified by PCR from pBabe-PURO-LITG (Dr. M. Klein, AG Jacobs, Max Planck Institute for Metabolism Research, Cologne, Germany) using the following primers (NheI restriction site in bolt):

Forward 5'-CGGAT**GCTAGC**GAGAGCTTGGCA-3'

Reverse 5'-TTGAT**GCTAGC**TCCGGGGTACGAAG-3'

After restriction with NheI, fLuc-IRES was inserted into the NheI restriction site of pLKO.1-CMV-mCherry. Sequencing revealed the right orientation of the insert sequence.

2.3 Lentiviral vector particle production

Lentiviral vector particles were produced as described elsewhere (Palm et al., 2013, Viel et al., 2013). In brief, after medium exchange to fresh DMEM without serum and antibiotics, HEK293T cells were transfected with a mixture of three plasmids. 2.6 µg of pLKO.1-CMV-LIC plasmid was mixed with 3.8 µg of a second-generation packaging plasmid (pCMV-dR8.2 dvpr; provided by Dr. R. Thomas (Max Planck Institute for Metabolism Research, Cologne, Germany)) and 0.76 µg of a plasmid encoding the glycoprotein G of vesicular stomatitis virus (pCMV-VSV-G; Dr. R. Thomas) in 250 µl OptiMEM I Reduced Serum Media (Gibco). 7.16 µl Plus Reagent (Life Technologies, Carlsbad, CA, USA) were added, solution was vortexed and incubated for 10 min at room temperature (RT). In a 24 well plate, 250 µl OptiMEM I Reduced Serum Media was mixed with 21.7 µl Lipofectamine LTX (Life Technologies) and 250 µl of the DNA Mix. After 30 min incubation at RT, the transfection mix was added to the cells. Supernatant was replaced on the next day by DMEM supplemented with 10% FBS without P/S. Supernatants were harvested and pooled on days 2 and 3, cleared through a 0.45 µm filter and vector particles were concentrated by low-speed centrifugation (5 h, 26000 g) at 4°C (Heraeus Biofuge Stratos, Thermo Fisher Scientific, Waltham, MA, USA). After resuspension in DMEM supplemented with 8 µg/ml polybrene

This article is protected by copyright. All rights reserved.

Accepted Article

(hexadimethrine bromide; Sigma-Aldrich, St. Louis, MO, USA), 500-fold concentrated vector particles were stored at -80°C.

2.4 Titration of lentiviral particles

For titration of lentiviral particles, 0.8 x 10^4 Gli36ΔEGFR cells were seeded in black 96-well plates with transparent bottom in 200 µl of DMEM supplemented with 10% FBS and 1x P/S. After cells reached confluence, medium was replaced by serial dilutions of concentrated viral particles in DMEM supplemented with 10% FBS, 1x P/S and 8 µg/ml polybrene. The next day, medium was replaced and mCherry positive cells were counted the day after (AxioCam MRm, Carl Zeiss, Oberkochen, Germany). The mean transduction efficiency was $1.7x10^5$ transducing units/µl.

2.5 Animal experiments

All animal experiments were performed in accordance with the German laws for animal protection and were approved by the local bureau for animal care (LANUV, Landesamt für Natur, Umwelt und Verbraucherschutz Nordrhein-Westfalen). C57Bl6 and FVB mice (Janvier, Saint-Berthevin, France) were housed at constant temperature (23°C) and relative humidity (40%), under a 12h light / 12h dark schedule. Mice were given *ad libitum* access to food and water.

2.6 6-OHDA Parkinson´s disease model

For stereotactic 6-OHDA injections, C57Bl6 mice (11-15 weeks of age) were anaesthetised with 150 mg/kg ketamine and 6 mg/kg xylazine (i.p.) and fixed into a stereotactic frame (Kopf Instruments, Tujunga, CA, USA). A small skin incision was made and a hole was drilled into the skull. The needle was placed in position and after 1 min, 2 µl 5 mg/ml 6-

This article is protected by copyright. All rights reserved.

Accepted Article

OHDA (Sigma-Aldrich) in 0.01% ascorbic acid (Carl Roth, Karlsruhe, Germany) and 0.9% NaCl (Carl Roth) or vehicle (0.01% ascorbic acid in 0.9% NaCl) was injected into the left SN using a Hamilton 7005KH 5 µl syringe. The syringe was kept in place for 5 min in order to allow the solution to diffuse into the surrounding tissue and was then retracted slowly. The following stereotactic coordinates in relation to bregma were used for the SN: lateral (La) -1.5 mm, anterior-posterior (AP) -3.0 mm, dorsal-ventral (DV) -4.4 mm.

2.7 Injection of lentiviral particles

For the stereotactic injection of lentiviral particles, FVB mice (6-7 weeks old) were anesthetised with 180 mg/kg ketamine and 9.6 mg/kg xylazine (i.p.). The surgical procedure is described above. The stereotactic coordinates for the SVZ were La -1.4 mm, AP +0.8 mm, DV -2.5 mm (-2.7 mm). The two coordinates for DV indicate, that the needle was placed at DV -2.7 mm, kept in place for one min, retracted to DV -2.5 mm and kept in place for one min before 2 µl of concentrated lentivirus particle solution was injected.

2.8 Single Photon Emission Computed Tomography (SPECT)

Animals were anaesthetised with 1.5% isoflurane (Abbott Animal Health, Illinois, USA) in 100% O_2 and the lateral tail vein was cannulated using a 26 Ga catheter (Vasculon Plus, BD, Heidelberg, Germany) connected to a 15 cm polyethylene tubing (27 Ga, Smith Medical, Kent, UK). 16 MBq [^{123}I]Ioflupane (N-ω-fluoropropyl-2β-carbomethoxy-3β-(4-[^{123}I]iodophenyl)nortropane, DaTscan^{TM}, GE Healthcare, Chalfont St Giles, GB) were injected i.v. and a 15 min SPECT scan was conducted 60 min post injection (p.i.) in a combined SPECT/CT imaging system (NanoSPECT/CT preclinical camera; Mediso Medical Imaging Systems, Budapest, Hungary), followed by a CT acquisition for acquiring anatomical information. Images were reconstructed by an ordered-subsets expectation maximization algorithm software (HiSPECT™; SciVis GMBH, Göttingen, Germany).

This article is protected by copyright. All rights reserved.

Accepted Article

Accepted Article

2.9 SPECT data analysis

Image data analysis of SPECT/CT data was performed using the Inveon™ Research Workspace software package (Siemens Healthcare, Erlangen, Germany). Volumes of interest (VOIs) in equal size and orientation were applied in order to quantify tracer uptake in left and right striatum as well as in the cerebellum. A 50% threshold of the VOI maximum was applied to the VOI for right striatum, and the resulting $VOI_{50\%right}$ was mirrored to the left brain hemisphere in order to quantify the left striatum ($VOI_{50\%left}$). [^{123}I]Ioflupane uptake was quantified as mean specific tracer uptake ([mean uptake $striatum_{50\%left/right}$ – mean uptake cerebellum] / mean uptake cerebellum) and the specific uptake ratio left/right was calculated. Representative images show SPECT and magnetic resonance (MR) images that were co-registered using the contour of the mouse skull.

2.10 Positron emission computed tomography (PET)

Radiosynthesis of [^{18}F]DPA-714 (*N*,*N*-diethyl-2-(2-(4-(2-[^{18}F]fluoroethoxy)phenyl)-5,7-dimethylpyrazolo[1,5-a]pyrimidin-3-yl)acetamide) was conducted as described elsewhere (Damont et al., 2008, James et al., 2008). Animals were anaesthetised with 1.5% isoflurane (Abbott Animal Health) in 100% O_2 and the lateral tail vein was cannulated as described above. PET studies were performed on a high resolution small animal scanner (32 module quadHIDAC, Oxford Positron Systems Ltd., Oxford, U.K.). Data reconstruction was performed using a one-pass listmode EM algorithm (EMrecon) (Kösters et al., 2011). Animals were injected with 10 MBq [^{18}F]DPA-714 i.v. and images were acquired 45-75 min p.i.. Following the PET acquisition, the animal bed was transferred to the CT scanner (Inveon, Siemens Healthcare) for acquiring anatomical information. The CT images were co-registered to PET images using 3 spheres (Acros Organics, Geel, Belgium) rinsed in radiotracer prior to image acquisition as landmarks on the animal bed.

This article is protected by copyright. All rights reserved.

Accepted Article

2.11 Magnetic resonance imaging (MRI)

Mice were anaesthetised with 1.5% isoflurane (DeltaSelect; Dreieich, Germany) in O_2/compressed air, 30/70 1L/min. MRI was performed with a 9.4 T small animal MR scanner with 20 cm bore size (Bio-Spec 94/20; Bruker BioSpin MRI GmbH, Ettlingen, Germany), operated with the ParaVision 5.1 software (Bruker BioSpin MRI GmbH). Using a helium-cooled cryoprobe (Bruker BioSpin MRI GmbH), we obtained anatomical 2D T2w RARE brain images in three imaging planes (TR/TE 3000-5000/50, 12-28 slices, slice thickness 0.5 mm, field of view 2 cm^2, matrix 256^2, in plane resolution 78 μm^2).

2.12 PET data analysis

PET and MR image data were analysed using VINCI software (Vollmar et al., 2004). Fusion of PET and CT images was performed using the landmark tool of the VINCI software and PET/CT and MR images were co-registered using the contour of the mouse skull. Co-registered images were matched to a mouse brain template generated from the Swanson mouse brain atlas (Swanson, 2001) and VOIs for SN and striatum were defined based on the brain atlas. Quantification is based on mean tracer uptake values for the respective VOIs. The VOI for the right unlesioned striatum was used as background VOI.

2.13 Bioluminescence imaging (BLI)

After virus injection, BLI was performed on a weekly basis using the IVIS Spectrum Imaging System and Living Image 4.0 software (PerkinElmer, Waltham, MA, USA). The day before measurement, fur on the head was removed using depilatory cream (Pilca) under isoflurane (Abbott Animal Health) anaesthesia. Mice were injected i.p. with 300 mg/kg D-luciferin in phosphate buffered saline (PBS) without calcium and magnesium (PAA Laboratories). 3 min post D-luciferin injection, mice were anaesthetised with 2.5% isoflurane in 100% oxygen and

This article is protected by copyright. All rights reserved.

placed in the imaging system before two 10 min time frames were recorded at 8 and 18 min p.i. (field of view (FOV): B, subject height 1.5 cm, binning: 4, f/stop: 1). Grayscale photographic images and bioluminescence colour images were superimposed. Regions of interest were drawn for the right and left SVZ and OB to determine the signal intensity (Average Radiance [p/s/cm^2/sr]).

2.14 Immunohistochemistry

Mice were deeply anaesthetised with 5% isoflurane and transcardially perfused with 0.9% NaCl followed by 4% paraformaldehyde (PFA). Brains were isolated and post-fixed over night in 4% PFA. After paraffin embedding, 5 µm thick coronal microtome sections were cut. Following deparaffinisation and rehydration, sections were boiled in citrate buffer (pH6, 25°C) for antigen retrieval and stained according to one of the subsequent protocols using primary antibodies against Tyrosine Hydroxylase (Chk α TH 1:1000; ab76442, Abcam, Cambridge, UK), Iba1 (Rb α Iba1 1:250; #019-19742, Wako Chemicals, Neuss, Germany), Doublecortin (Gp α Dcx 1:400; AB2253, Millipore, Billerica, MA, USA), GFAP (Chk α GFAP 1:1000; ab13970, Abcam) or TSPO (Rb α PBR 1:250; EPR5384, Novus Biologicals, Cambridge, UK).

Immunofluorescence staining: After washing with PBS and preincubation with blocking solution (4% goat serum, 0.25% Triton-X in PBS) for 20 min, sections were incubated with primary antibody in blocking solution at 4°C over night, washed with PBS and incubated with the respective secondary antibody (Alexa Fluor 488/555 1:800, Life Technologies) in blocking solution for 45 min at RT in a dark chamber. After washing with PBS, sections were incubated with 0.5 µg/ml DAPI (Carl Roth) in PBS for 7 min, washed again and mounted with Mowiol (Sigma-Aldrich).

This article is protected by copyright. All rights reserved.

Accepted Article

Immunoperoxidase staining: Blocking was performed with Peroxidase-blocking solution (S2023, Dako, Hamburg, Germany) for 10 min followed by washing with PBS. Sections were then incubated in primary antibody diluted in antibody diluent (S3022, Dako), washed in PBS, incubated with biotinylated secondary antibody (DSB-X™ Biotin Goat Anti-Chicken IgG 1:800, Life Technologies) in antibody diluent, washed in PBS and incubated with HRP-Streptavidin conjugate (1:600 in PBS, P0397, Dako) for 45 min. After final washing in PBS, sections were placed in 2% 3,3'-Diaminobenzidine (DAB), 0.0012% H_2O_2 until reaching a good staining intensity. Sections were counterstained with haematoxylin for 5-10 sec (1:3 in Aqua dest), dehydrated and mounted in entellan (Millipore).

2.15 Microscopy

Stained sections were analysed using a Nikon ECLIPSE Ni-E microscope operated by the NIS-Elements AR software. Z-Stacks (± 2 µm in 0.5 µm steps) were recorded and combined to a focused image using the extended depth of focus (EDF) function.

For quantification purposes, cells from 3 images from the respective region of every animal were manually counted.

2.16 Statistical analysis

Statistical analysis was performed in Sigma Plot 13.0 (Systat Software Inc, San Jose, CA, USA). SPECT data and $Iba1^+$ cell counts were analysed using a Two Way ANOVA followed by a Pairwise Multiple Comparison Procedure (Holm-Sidak Method). PET data were analysed using a Mann-Whitney Rank Sum Test. BLI data were analysed using a Two Way Repeated Measures ANOVA. For data analysed using ANOVA, values are shown as mean values (*M*) with standard deviation (*SD*). For data analysed using the Mann-Whitney Rank Sum Test, values are shown as median values (*Mdn*) with upper and lower percentiles. A *P*-value below 0.05 was considered as significant.

This article is protected by copyright. All rights reserved.

Accepted Article

Accepted Article

3. RESULTS

Neurodegenerative processes in PD were reported to be accompanied by neuroinflammatory processes, which potentially can both favour or reduce disease progression and regeneration. We therefore investigated neurodegeneration, neuroinflammation, and stem cell properties in the unilateral 6-OHDA injection mouse model for PD. The detailed experimental setup including the exact numbers of studied animals and the timing of the various imaging approaches is illustrated in supplementary Figure S2 and S3.

3.1 6-OHDA induced neurodegeneration

In order to ensure degeneration of dopaminergic nigrostriatal projections in 6-OHDA treated animals and integrity of the nigrostriatal system in vehicle injected animals, [^{123}I]Ioflupane-SPECT was performed at different time points post injection (Fig. 1a and supplementary Fig. S2). Tracer uptake in the left striatum was observed to be reduced in 6-OHDA treated (n_{d3} = 5; n_{d7} = 4; n_{d18} = 7) compared to vehicle injected (n_{d3} = 3; n_{d7} = 5; n_{d18} = 8) mice at all studied time points (Fig. 1 a & b), whereas tracer uptake in the right striatum did not change (Fig. 1c), indicating degeneration of ipsilateral striatal projections without compensation on the contralateral site. Both, left and right striatum, showed a very variable absolute tracer uptake between the different time points, which did not allow for statistical testing with a Two Way ANOVA due to violation of the equal variance assumption. As presynaptic dopamine transporter (DaT) levels can vary between individuals, and specific activities can vary between tracer syntheses, we calculated the ratio of the mean tracer uptake in the striatum left/right (Fig. 1d). The specific [^{123}I]Ioflupane uptake ratio between vehicle- and 6-OHDA-injected animals differed significantly (Two Way ANOVA, $F_{1,26}$ = 117.67, P < 0.001) and was significantly reduced in 6-OHDA treated compared to vehicle treated animals at all time points (d3: $M_{6\text{-OHDA}}$ = 0.08, $SD_{6\text{-OHDA}}$ = 0.30, M_{vehicle} = 0.96, SD_{vehicle} = 0.08, t = 6.34, P <

This article is protected by copyright. All rights reserved.

0.001; d7: $M_{6\text{-OHDA}}$ = 0.34, $SD_{6\text{-OHDA}}$ = 0.11, M_{vehicle} = 1.09, SD_{vehicle} = 0.06, t = 5.83, P < 0.001; d18: $M_{6\text{-OHDA}}$ = 0.09, $SD_{6\text{-OHDA}}$ = 0.12, M_{vehicle} = 0.77, SD_{vehicle} = 0.20, t = 6.94, P < 0.001; Pairwise Multiple Comparison Procedure, Holm-Sidak method). No statistically significant interaction between group and time point could be observed (Two Way ANOVA, $F_{2,26}$ = 0.68 , P = 0.52), suggesting that nigrostriatal degeneration is a fast process taking a maximal time of a few days to reach the final state of degeneration. Intranigral application of 6-OHDA induced a fast degeneration of axonal projections towards the striatum, which was also visible in histological stainings for tyrosine hydroxylase (TH), the rate-limiting enzyme in the synthesis of dopamine (Nagatsu et al., 1964). TH staining intensity was clearly reduced in the left striatum as well as numbers of TH^+ cell bodies in the left SN, compared to the unlesioned contralateral side (Fig. 2a & b). The observed amount of degeneration was comparable at all studied time points, again stressing the short time frame needed for neurodegeneration in this model.

3.2 Neuroinflammatory processes accompanying neurodegeneration

As several studies reported neuroinflammation accompanying degeneration of dopaminergic neurons in PD, we aimed to investigate the presence of neuroinflammation after 6-OHDA lesion. To assess this parameter, we performed PET with the TSPO ligand [^{18}F]DPA-714 at 7 (n_{vehicle} = 6; $n_{6\text{-OHDA}}$ = 7), 14 (n_{vehicle} = 12; $n_{6\text{-OHDA}}$ = 12) and 21 (n_{vehicle} = 11; $n_{6\text{-OHDA}}$ = 9) days post lesion (supplementary Fig. S2). Tracer uptake was clearly visible in the left SN as well as in the injection tract region (Fig. 3a). At 7 days post injection (dpi), tracer uptake was higher in the left SN, compared to right SN in 6-OHDA and vehicle treated animals, but without reaching statistical significance between both groups (Figure 4b, ratio SN_{left}/SN_{right}, $Mdn_{6\text{-OHDA}}$ = 1.29, Mdn_{vehicle} = 1.09, U = 12.0, P = 0.234; Mann-Whitney Rank Sum Test), pointing out enhanced inflammatory processes in both groups due to the injection procedure.

This article is protected by copyright. All rights reserved.

Accepted Article

At 14 days post injection (dpi), the signal-to-background ratio and the SN_{left}/SN_{right} ratio was increased in 6-OHDA lesioned compared to vehicle injected animals (Figure 4a & b), showing increased inflammation after neurotoxic degeneration (SN left/background: $Mdn_{6\text{-}OHDA}$ = 1.60, $Mdn_{vehicle}$= 1.26, U = 29.0, P = 0.014; SN left/right: $Mdn_{6\text{-}OHDA}$ = 1.27, $Mdn_{vehicle}$= 1.08, U = 36.0, P = 0.040; Mann-Whitney Rank Sum Test). This neuroinflammatory response abated 21 days post injection, as measured by not significantly altered signal to background and SN_{left}/SN_{right} ratios (SN left/background: $Mdn_{6\text{-}OHDA}$ = 1.28, $Mdn_{vehicle}$= 1.42, U = 39.0, P = 0.447; SN left/right: $Mdn_{6\text{-}OHDA}$ = 1.11, $Mdn_{vehicle}$= 1.17, U = 49.0, P = 1.0; Mann-Whitney Rank Sum Test).

The median left/right tracer uptake ratio for the striatum was comparable at day 7 and day 21 (Figure 3b & 4e), while it was slightly, but significantly, higher in the 6-OHDA lesioned striatum at day 14 (d7: $Mdn_{6\text{-}OHDA}$ = 1.08, $Mdn_{vehicle}$ = 1.01, U = 7.0, P = 0.051; *Mdn* d14: $Mdn_{6\text{-}OHDA}$ = 1.03, $Mdn_{vehicle}$ = 0.95, U = 31.0, P = 0.019; d21: $Mdn_{6\text{-}OHDA}$ = 0.98, $Mdn_{vehicle}$ = 1.01, U = 45.0, P = 0.761; Mann-Whitney Rank Sum Test).

As the injection procedure itself might cause increased inflammation and thereby influence quantification of tracer uptake in 6-OHDA vs. vehicle, we calculated the ratio injection tract/background and mean %ID tracer uptake in the injection tract at 7 ($n_{vehicle}$ = 6; $n_{6\text{-}OHDA}$ = 8) and 14 dpi ($n_{vehicle}$ = 9; $n_{6\text{-}OHDA}$ = 10) (Figure 4c & 4d). Due to advanced healing processes, the injection tract was not visible in all cases on day 21 in the MRI data and was therefore not quantified. Median tracer uptake in the injection tract did not differ significantly between 6-OHDA and vehicle injected brains (injection tract/background: d7: $Mdn_{6\text{-}OHDA}$ = 1.64, $Mdn_{vehicle}$ = 1.55, U = 18.0, P = 0.491; d14: $Mdn_{6\text{-}OHDA}$ = 1.49, $Mdn_{vehicle}$ = 1.49, U = 44.0, P = 0.967; %ID injection tract: d7: $Mdn_{6\text{-}OHDA}$ = 2.21, $Mdn_{vehicle}$ = 1.92, U = 19.0, P = 0.573; d14: $Mdn_{6\text{-}OHDA}$ = 1.89, $Mdn_{vehicle}$ = 1.63, U = 39.0, P = 0.653; Mann-Whitney Rank Sum Test), and was lower at d14 in general, but without reaching statistical significance.

This article is protected by copyright. All rights reserved.

Accepted Article

3.3 Histological analysis of microglial and astrocytic markers

We performed immunohistological stainings of SN and striatum for the microglial markers ionized calcium-binding adapter molecule 1 (Iba1) and TSPO, as well as for the astrocytic marker glial fibrillary acidic protein (GFAP) at 7, 14 and 21 dpi. Increased staining for $Iba1^+$ microglia was observed in the ipsilateral 6-OHDA-injected SN compared to the vehicle injected SN at all time points (Fig. 5a). The vehicle-injected SN displayed a certain amount of microgliosis, but without reaching the magnitude of the 6-OHDA condition. A peak in $Iba1^+$ microgliosis in the SN could be observed at day 14 post lesion. Microglia in the lesioned SN displayed an activated phenotype, as determined by increased cell body size and reduced ramifications (arrows in Fig. 5a). TSPO staining displayed the same regional patterning as Iba1 staining, while the staining was speckled over the cell body, prohibiting determination of the cell morphology (Fig. 5b). Astrogliosis, as shown by GFAP positivity, was persistent over time in the ipsilateral SN in 6-OHDA injected animals, but also observed in the ipsilateral SN of vehicle injected mice, indicating the role of astrocytes in wound healing (Fig. 5b).

TSPO staining was barely detectable in the ipsilateral striatum of 6-OHDA and vehicle injected animals, suggesting weak or no activation of striatal microglia. In the ipsilateral striatum of 6-OHDA lesioned animals, Iba1 staining was unchanged (Figure 5 c, e-f) and the left/right ratio of $Iba1^+$ cells was not significantly different between 6-OHDA and vehicle condition (Two Way ANOVA, $F_{1,15} = 3.737$, $P = 0.072$). In contrast, increased numbers of $GFAP^+$ cells were observed (Figure 5d), compared to striatum of vehicle injected specimen. Likewise, vehicle injection led to a slight increase in $GFAP^+$ cells compared to the contralateral site, but not to the same extent as after 6-OHDA injection.

This article is protected by copyright. All rights reserved.

3.4 Effect of neurodegeneration and –inflammation on neural stem cell proliferation and migration

In order to study the effect of neurodegeneration and neuroinflammation on neural stem cell (NSC) proliferation and migration in the unilateral 6-OHDA PD model, we first established injections of virus particles into the SVZ of FVB mice (the experimental setup is illustrated in supplemental Fig. S3). FVB mice were used because pigmented fur and skin of C57Bl6 do not allow for reliable quantification of optical imaging data due to light absorption and scattering. The plasmid used for production of lentiviral particles encodes mCherry and firefly luciferase protein and is driven by a cytomegalovirus (CMV) promoter (supplemental Fig. S1). BLI was conducted weekly in order to follow migration of infected neuroblasts, and proliferation and migration of progeny of infected NSCs in the same animal over time. One week post injection, BLI signal was detected at the site of injection in n = 24 out of 24 animals (100 %), but could not be quantified accurately due to remaining fur. At two to four weeks post injection, signals showed anterior extension in 12 out of 24 animals (50 %), demonstrating migration of labelled neuroblasts towards the OB (Fig. 6a). Animals which showed no anterior light signal extension were excluded from the study as virus particles in these cases failed to infect progenitor cells probably due to mislocated injections. Over time, the OB/SVZ changes significantly (Figure 6c; One Way Repeated Measures ANOVA, $F_{5,40}$ = 8.62, $P < 0.001$) and from week 5 post virus injection on, the mean OB/SVZ ratio was significantly higher compared to week 2 (Holm-Sidak Pairwise Multiple Comparison; week 5 vs. week 2: t = 3.33, P = 0.021; week 6 vs. week 2: t = 4.36, P = 0.001; week 7 vs. week 2: t = 5.65, $P < 0.001$) clearly showing signal accumulation in the OB over time. At 7.5 weeks post virus injection, 6-OHDA and vehicle injections into the SN were performed ($n_{\text{6-OHDA}}$ = 5, n_{vehicle} = 4) and weekly measurements were performed for additional 6 weeks (Fig. 6b). We used the OB/SVZ ratio for quantification in order to correct for fluctuations in total signal

This article is protected by copyright. All rights reserved.

Accepted Article

which originate from varying intraperitoneal absorption dynamics between different substrate injections. In order to correct for individual differences in signal distribution, the relative signal change compared to the mean value of the two measurements before lesion was computed (Fig. 6d & e).The absolute OB signal, SVZ signal, and OB/SVZ signal ratio is in addition displayed in supplemental Figure S4. After lesion induction, no significantly different mean SVZ/OB ratio change (Fig. 6e) in the 6-OHDA group was observed compared to the vehicle group (Two Way Repeated Measures ANOVA, $F_{1,42} = 0.0962$, $P = 0.765$). The mean OB signal change (Fig. 6d) showed high intra-individual differences and did not fulfil the equal variance assumption of the ANOVA (Shapiro-Wilk, $P = 0.03$).

Degeneration of dopaminergic neurons in the 6-OHDA lesioned SN and integrity of dopaminergic neurons in the vehicle-injected SN was validated after the final BLI acquisition by immunohistochemistry for TH in all animals included in the BLI data analysis (data not shown).

3.5 Histological analysis of neural progenitor cells post 6-OHDA lesion

As the detection of very small alterations in progenitor cell migration is challenging employing BLI, we additionally analysed sections from C57Bl6 mouse SVZ at different time points post intranigral 6-OHDA/vehicle injection. As a marker for neurogenesis, we used Doublecortin (Dcx, Fig. 7). Dcx is a microtubule-associated protein transiently expressed in neuronal progenitor cells and immature neurons (Brown et al., 2003) mainly in SVZ, dentate gyrus, rostral migratory stream and OB. Visual inspection at 4, 8, 15 and 21 days post lesion indicates no difference in Dcx staining between the contra- and ipsilateral SVZ of 6-OHDA lesioned and vehicle injected animals, leading to the assumption that neuroblast generation is not affected by the pathophysiological changes in the 6-OHDA lesioned brain (Fig. 7). Furthermore, only single or no Dcx^+ cells were observed at more lateral positions of the striatum.

This article is protected by copyright. All rights reserved.

Accepted Article

4. DISCUSSION

This study sought to shed light on the complex interplay of neurodegeneration, neuroinflammation and neurogenesis in the unilateral intranigral 6-OHDA-injection model of Parkinson's disease.

Employing [^{123}I]Ioflupane-SPECT, we observed significantly reduced tracer binding in the lesioned striatum at 3, 7, and 18 days post lesion, indicating degeneration of ipsilateral striatal projections with loss of DaTs in a time frame of several days.

At 14 dpi, increased uptake ratios for [^{18}F]DPA-714 were measured in 6-OHDA lesioned compared to vehicle injected animals via PET. Striatal DPA-714 uptake ratios were comparable at day 7 and day 21, while they were slightly, but significantly, higher in the 6-OHDA lesioned striatum at day 14.

Histological analysis revealed a peak in Iba1^{+} microgliosis in the SN at day 14 post lesion, but no increased numbers of microglia in the striatum. Astrogliosis, as shown by GFAP positive staining, was persistent over time in the ipsilateral SN in 6-OHDA injected animals, but it was also observed in the ipsilateral SN of vehicle injected mice. Increased astrogliosis was also detectable in the ipsilateral striatum of 6-OHDA injected mice.

We could visualise migration of labelled neuroblasts towards the OB using BLI after virus injection, with a stable signal distribution at week 7. After 6-OHDA lesion, no significantly different OB or OB/SVZ signal was observed compared to the vehicle group. Histological analysis of Dcx expression in the SVZ underlined unaltered neuroblast generation.

4.1 Intranigral 6-OHDA-injection induces a fast degeneration of the nigrostriatal system

Induction of dopaminergic neurodegeneration by 6-OHDA injection into the SN allows the study of SVZ neurogenesis after degeneration of striatal projections without direct influence from the damage caused by the injection procedure itself. After intranigral injection, we

This article is protected by copyright. All rights reserved.

Accepted Article

observed degeneration of dopaminergic neurons taking place over several days, as also described after SN or medial forebrain bundle (MFB) neurotoxin administration (Jeon et al., 1995, Walsh et al., 2011). The major portion of dopaminergic neurons in the SN was reported to die during the first 10 days post lesion in rats, while fibre degeneration in the striatum was observed between day 1 and 7 in the striatum (Jeon et al., 1995). We could observe this reduction in dopaminergic innervation as a strong reduction in DaT ligand accumulation in the ipsilateral striatum and reduced TH staining intensity at early and at late time points. DaT density in the striatum is directly correlated with the number of dopaminergic cell bodies in the SN, making Ioflupane-SPECT an excellent read-out for dopaminergic neurodegeneration in the SN (Bäck et al., 2013). The detected amount of tracer uptake in the contralateral striatum was comparable at all time points, indicating that the contralateral site does not compensate for loss of innervation on the ipsilateral site.

4.2 Degeneration of dopaminergic cell bodies is accompanied by acute neuroinflammation

Degeneration of dopaminergic neurons was reported to be accompanied by neuroinflammatory processes in patients (Imamura et al., 2003, McGeer et al., 1988), and in animal models of PD (Akiyama and McGeer, 1989, Czlonkowska et al., 1996). Our *in vivo* PET study showed an acute increase in TSPO-ligand accumulation at the direct lesion site in 6-OHDA compared to vehicle injected animals, while tracer accumulation in the striatum was significantly, but very slightly ($Mdn_{\text{6-OHDA}}$ = 1.03, Mdn_{vehicle} = 0.95) increased. However, visual inspection of the PET datasets as well as analysis of the corresponding immunohistochemistry for Iba1 and TSPO gave no evidence for significant microglial activation in the striatum. We would expect to observe left/right ratios of 1.0 in control animals and > 1.0 in animals with increased inflammation of the ipsilateral side, while we

This article is protected by copyright. All rights reserved.

Accepted Article

observed a value of < 1.0 in the control condition. Most likely, the measured values are in the range of the normally occurring variations in tracer uptake and the observed *P*-value of below 0.05 is coincidentally and has no biological relevance.

As numbers of $Iba1^+$ cells were unchanged in the striatum and TSPO reactivity was barely detectable, our data indicate, that degeneration of nerve terminals is no trigger for microglia activation, while degenerating cell bodies strongly trigger inflammatory cells.

In line with this, previous studies proved increased microglia activation at the direct 6-OHDA lesion site in the SN, but only weak or missing microglia activation in the striatum (Kitamura et al., 2010, Walsh et al., 2011). In contrast, intrastriatal injections led to increased inflammation at the primary and secondary lesion site (Cicchetti et al., 2002, He et al., 2001, Maia et al., 2012). Concerning the time course of microglia activation, a peak in microglia activation in the SN at 2 weeks post lesion was reported for intrastriatal 6-OHDA injection in rats (Cicchetti et al., 2002, Maia et al., 2012) and mice (He et al., 2001), further underlining our observation that microglia activation is an acute process in this PD model. If microglia activation appears only after the neurodegenerative process is complete, or already during the neurodegenerative process remains elusive. Due to the invasiveness of the intranigral injection, we cannot distinguish between early degeneration-induced neuroinflammation and the inflammatory response caused by the injection procedure itself. Therefore, we cannot rule out, that inflammation is already present during the neurodegenerative process and not only after completion of this process. In addition, blood brain barrier (BBB) integrity might be crucial for the quantification of tracer uptake, as the mechanical damage caused by the injection procedure certainly increases BBB permeability early after lesion. However, this effect will influence tracer uptake in both, vehicle and 6-OHDA-lesioned animals and therefore does not interfere with our analysis. Moreover, our histological findings confirmed our PET imaging findings. As the variability of tracer uptake and inter-individual differences

This article is protected by copyright. All rights reserved.

Accepted Article

are major challenges for PET quantification, longitudinal imaging and injection of 6-OHDA and vehicle in the same animal might reduce group variability in future studies. However, this experimental setup lacks the possibility for direct histological validation and does not allow the evaluation of the integrity of the nigrostriatal system following vehicle injection by *in vivo* imaging.

4.3 Degeneration of the nigrostriatal system leads to persistent astrogliosis

Despite the missing striatal microgliosis, we found severe and persistent astrogliosis in SN and striatum after 6-OHDA lesion, demonstrated by GFAP immunoreactivity. Increased numbers of nigral and striatal astrocytes were previously shown in several models of 6-OHDA administration (Akiyama and McGeer, 1989, Maeda et al., 2008, Sheng et al., 1993). Striatal astrocytes might derive from resident astrocytes that undergo de-differentiation (Buffo et al., 2008), as well as from SVZ progenitor cells (Levison and Goldman, 1993). After intraventricular application of 6-OHDA in rats, numbers of $Ki67^{+}$ proliferating cells were reported to be unchanged in the SVZ, while proliferation was increased in striatum and cortex (Wachter et al., 2010). These proliferating cells did not co-localise with the microglial marker Iba1, but with the astrocytic marker GFAP, identifying them as locally proliferating astrocytes. Persistent astrogliosis potentially reflects residual astrocytic scarring, which remains after the phagocytotic activity has been completed (Akiyama and McGeer, 1989).

4.4 Subventricular neurogenesis is unaffected by striatal deafferentation

Previous studies implemented lentiviral *in vivo* transduction of neural stem cells with constructs encoding for firefly luciferase as a tool to follow migration of progenitor cells in the SVZ – OB axis and showed that sensitivity of this method is sufficient to detect alterations in neurogenesis caused by bone derived neurotrophic factor overexpression

This article is protected by copyright. All rights reserved.

Accepted Article

(Reumers et al., 2008) or cuprizone treatment (Guglielmetti et al., 2013). We established injections of LV-CMV-LIC into the SVZ and could follow progenitor cell migration towards the OB over time using BLI. Neurotoxin injection into the left SN led to unchanged relative OB/SVZ signal ratios. However, we observed a smaller absolute OB/SVZ ratio in 6-OHDA lesioned compared to vehicle injected animals. In fact, this difference was already present prior to lesion, indicating that it is independent of the lesion procedure, and is not present in the quantification of the OB/SVZ ratio relative to the mean value of the two last measurements before lesion. Taken together, our data suggest unaffected neural progenitor cell migration in FVB mice following 6-OHDA lesion. Our histological analysis of Dcx^+ cells in the SVZ of C57Bl6 mice further supports this *in vivo* imaging based observation. These findings are in line with results from intrastriatal 6-OHDA injections in rats, which led to increased numbers of proliferating cells in the SVZ, without affecting numbers of Dcx^+ cells (Aponso et al., 2008). The characterisation of these new born cells revealed high expression of the astrocytic marker GFAP, indicative of lesion-induced astrogenesis.

Additionally, intranigral injection of 6-OHDA in mice was reported to lead to no changes in striatal 5-Ethynyl-2'-deoxyuridine (EdU) incorporating cells or SVZ neuroblasts, while inhibition of neuroinflammation by minocycline led to increased EdU^+ cells and neuroblasts migrating deeply into the striatum in 6-OHDA but not vehicle injected animals (Worlitzer et al., 2012). On the other hand, a 40% reduction in proliferating neural precursors in the SVZ was reported after 6-OHDA lesion of the MFB and SN in mice (Baker et al., 2004). It is important to notice that these mice received double 6-OHDA injections which led to a nearly complete dopamine deprivation. As neural progenitor cells might be dopamine-sensitive (O'Keeffe et al., 2009), a complete loss of striatal dopamine could affect cell proliferation in a different manner than a reduction in dopamine content. Based on our findings and the existing literature, neurodegeneration and neuroinflammation do not seem to affect

This article is protected by copyright. All rights reserved.

Accepted Article

neuroblast generation, but might affect the proliferation of progenitor cells and in parallel shift the ratio of neuro-/gliogenesis towards gliogenesis, in particular astrogenesis. One possible explanation for the lack of neurogenesis coming along with increased progenitor cell proliferation might be the lack of stimulatory cues and a restrictive microenvironment (Raponi et al., 2007).

4.5 Conclusion

To our knowledge, this is the first study which covered *in vivo* imaging of neurodegeneration, neuroinflammation, and neurogenesis in the SVZ-OB axis in the same Parkinson's disease mouse model. We were able to validate our imaging findings with extensive histology for TH^+ dopaminergic neurons, $GFAP^+$ astrocytes, as well as $TSPO^+$ and/or $Iba1^+$ microglia, showing that *in vivo* imaging is able to pick up changes in neurodegeneration and neuroinflammation following 6-OHDA lesion. After our careful immunohistochemical analysis, these methods can now be used to perform longitudinal studies, thereby reducing interindividual differences while at the same time reducing the numbers of animals. We found that activation of microglia is an acute process coming along with the degeneration of dopaminergic cell bodies, and potentially reinforcing neuronal loss. Dopaminergic deafferentation of the striatum has no impact on the generation of Dcx^+ neuroblasts in the SVZ, but strongly triggers chronic astrogliosis. Our results suggest, that early anti-inflammatory treatment might reduce neuronal loss in the SN, while at later time points, treatments that increase neural progenitor cell proliferation and shift the fate of newly generated cells towards a neuronal phenotype could be a favourable approach.

This article is protected by copyright. All rights reserved.

Accepted Article

Accepted Article

ACKNOWLEDGEMENTS

The authors thank M. Duffy and S. Schelhaas for proof reading and C. Bätza, S. Bouma, F. Breuer, W. Gottschlich, C. Gräf, I. Hoppe, M. Kattenbeck, S. Köster, C. Möllmann, R. Priebe, and D. Reinhard for their excellent technical support.

The research leading to these results has received funding from the Interdisciplinary Centre for Clinical Research (IZKF); Münster; Germany (project SchwJ3/001/11 and Core Unit PIX) and the European Union's Seventh Framework Programme (FP7/2007-2013) under grant agreement n° 278850 (INMiND). The authors declared no conflict of interest.

AUTHOR CONTRIBUTIONS

IBF conducted the experiments, designed the figures, and drafted the manuscript. TV conducted the experiments and drafted the manuscript. MMW established the 6-OHDA lesion model. FMC was involved in BLI measurements and analysis. AV assisted the SPECT studies and analysis. AF synthesized [^{18}F]DPA-714. LW and CF designed and performed the MRI studies. FD helped in setting up the [^{18}F]DPA-714 synthesis in Münster. MTK advised on surgery and histology. KS and SH supported the PET and SPECT imaging and analysis. JCS and AHJ designed the study, were involved in data interpretation, and drafted the manuscript.

ABBREVIATIONS

%ID	percent injected dose
[^{18}F]DPA-714	N,N-diethyl-2-(2-(4-(2-[18F]fluoroethoxy)phenyl)-5,7-dimethylpyrazolo[1,5-a]pyrimidin-3-yl)acetamide)
6-OHDA	6-hydroxydopamine
BBB	blood brain barrier

This article is protected by copyright. All rights reserved.

BLI	bioluminescence imaging
CMV	cytomegalovirus
d	day
DaT	presynaptic dopamine transporter
Dcx	doublecortin
dpi	days post injection
EdU	5-Ethynyl-2'-deoxyuridine
GFAP	glial fibrillary acidic protein
Iba1	ionized calcium-binding adapter molecule 1
MFB	medial forebrain bundle
MPTP	1-Methyl-4-phenyl-1,2,3,6-tetrahydropyridin
MRI	Magnetic resonance imaging
NSC	neural stem cell
OB	olfactory bulb
PD	Parkinson's disease
PET	positron emission tomography
SGZ	subgranular zone
SN	substantia nigra
SPECT	single photon emission computed tomography
SVZ	subventricular zone
TH	tyrosine hydroxylase
TSPO	translocator protein

Accepted Article

This article is protected by copyright. All rights reserved.

Accepted Article

REFERENCES

Akiyama H, McGeer PL (1989) Microglial response to 6-hydroxydopamine-induced substantia nigra lesions. *Brain Res* 489:247–53.

Aponso PM, Faull RLM, Connor B (2008) Increased progenitor cell proliferation and astrogenesis in the partial progressive 6-hydroxydopamine model of Parkinson's disease. *Neuroscience* 151:1142–53.

Bäck S, Raki M, Tuominen RK, Raasmaja A, Bergström K, Männistö PT (2013) High correlation between in vivo [123I]β-CIT SPECT/CT imaging and post-mortem immunohistochemical findings in the evaluation of lesions induced by 6-OHDA in rats. *EJNMMI Res* 3:46.

Baker SA, Baker KA, Hagg T (2004) Dopaminergic nigrostriatal projections regulate neural precursor proliferation in the adult mouse subventricular zone. *Eur J Neurosci* 20:575–9.

Bastos GN, Moriya T, Inui F, Katura T, Nakahata N (2008) Involvement of cyclooxygenase-2 in lipopolysaccharide-induced impairment of the newborn cell survival in the adult mouse dentate gyrus. *Neuroscience* 155:454–62.

Booij J, Andringa G, Rijks LJ, Vermeulen RJ, Bruin KD, Boer GJ, Janssen AG, Royen EAV (1997a) [123I]FP-CIT binds to the dopamine transporter as assessed by biodistribution studies in rats and SPECT studies in MPTP-lesioned monkeys. *Synapse* 27:183–90.

Booij J, Tissingh G, Boer GJ, Speelman JD, Stoof JC, Janssen AG, Wolters EC, van Royen EA (1997b) [123I]FP-CIT SPECT shows a pronounced decline of striatal dopamine transporter labelling in early and advanced Parkinson's disease. *J Neurol Neurosurg Psychiatr* 62:133–40.

Brown JP, Couillard-Després S, Cooper-Kuhn CM, Winkler J, Aigner L, Kuhn HG (2003) Transient expression of doublecortin during adult neurogenesis. *J Comp Neurol* 467:1–10.

This article is protected by copyright. All rights reserved.

Accepted Article

Buffo A, Rite I, Tripathi P, Lepier A, Colak D, Horn AP, Mori T, Götz M (2008) Origin and progeny of reactive gliosis: A source of multipotent cells in the injured brain. *Proc Natl Acad Sci U.S.A.* 105:3581–6.

Chen MK, Guilarte TR (2008) Translocator protein 18 kDa (TSPO): molecular sensor of brain injury and repair. *Pharmacol Ther* 118:1–17.

Cicchetti F, Brownell AL, Williams K, Chen YI, Livni E, Isacson O (2002) Neuroinflammation of the nigrostriatal pathway during progressive 6-OHDA dopamine degeneration in rats monitored by immunohistochemistry and PET imaging. *Eur J Neurosci* 15:991–8.

Cosenza-Nashat M, Zhao ML, Suh HS, Morgan J, Natividad R, Morgello S, Lee SC (2009) Expression of the translocator protein of 18 kDa by microglia, macrophages and astrocytes based on immunohistochemical localization in abnormal human brain. *Neuropathol Appl Neurobiol* 35:306–28.

Czlonkowska A, Kohutnicka M, Kurkowska-Jastrzebska I, Czlonkowski A (1996) Microglial reaction in MPTP (1-methyl-4-phenyl-1,2,3,6-tetrahydropyridine) induced Parkinson's disease mice model. *Neurodegeneration* 5:137–43.

Damont A, Hinnen F, Kuhnast B, Schöllhorn-Peyronneau MA, James M, Luus C, Tavitian B, Kassiou M, Dollé F (2008) Radiosynthesis of [18F]DPA-714, a selective radioligand for imaging the translocator protein (18 kDa) with PET. *Journal of Labelled Compounds and Radiopharmaceuticals* 51:286–92.

Damont A, Roeda D, Dollé F (2013) The potential of carbon-11 and fluorine-18 chemistry: illustration through the development of positron emission tomography radioligands targeting the translocator protein 18 kDa. *J Labelled Comp Radiopharm* 56:96–104.

Dollé F, Luus C, Reynolds A, Kassiou M (2009) Radiolabelled molecules for imaging the

This article is protected by copyright. All rights reserved.

translocator protein (18 kDa) using positron emission tomography. *Curr. Med. Chem.* 16:2899–923.

Ekdahl CT, Claasen JH, Bonde S, Kokaia Z, Lindvall O (2003) Inflammation is detrimental for neurogenesis in adult brain. *Proc Natl Acad Sci U.S.A.* 100:13632–7.

Fearnley JM, Lees AJ (1991) Ageing and Parkinson's disease: substantia nigra regional selectivity. *Brain* 114 (Pt 5):2283–301.

Giatzakis C, Papadopoulos V (2004) Differential utilization of the promoter of peripheral-type benzodiazepine receptor by steroidogenic versus nonsteroidogenic cell lines and the role of Sp1 and Sp3 in the regulation of basal activity. *Endocrinology* 145:1113–23.

Guglielmetti C, Praet J, Rangarajan JR, Vreys R, Vocht ND, Maes F, Verhoye M, Ponsaerts P, der Linden AV (2013) Multimodal imaging of subventricular zone neural stem/progenitor cells in the cuprizone mouse model reveals increased neurogenic potential for the olfactory bulb pathway, but no contribution to remyelination of the corpus callosum. *Neuroimage* .

He Y, Appel S, Le W (2001) Minocycline inhibits microglial activation and protects nigral cells after 6-hydroxydopamine injection into mouse striatum. *Brain Res* 909:187–93.

Höglinger GU, Rizk P, Muriel MP, Duyckaerts C, Oertel WH, Caille I, Hirsch EC (2004) Dopamine depletion impairs precursor cell proliferation in Parkinson disease. *Nat Neurosci* 7:726–35.

Imamura K, Hishikawa N, Sawada M, Nagatsu T, Yoshida M, Hashizume Y (2003) Distribution of major histocompatibility complex class II-positive microglia and cytokine profile of Parkinson's disease brains. *Acta Neuropathol* 106:518–26.

Jacobs AH, Tavitian B (2012) Noninvasive molecular imaging of neuroinflammation. *J. Cereb. Blood Flow Metab.* 32:1393–415.

This article is protected by copyright. All rights reserved.

Accepted Article

Accepted Article

James ML, Fulton RR, Vercoullie J, Henderson DJ, Garreau L, Chalon S, Dolle F, Costa B, Selleri S, Guilloteau D, Kassiou M (2008) DPA-714, a new translocator protein-specific ligand: synthesis, radiofluorination, and pharmacologic characterization. *J Nucl Med* 49:814–22.

Jeon BS, Jackson-Lewis V, Burke RE (1995) 6-Hydroxydopamine lesion of the rat substantia nigra: time course and morphology of cell death. *Neurodegeneration* 4:131–7.

Kitamura Y, Inden M, Minamino H, Abe M, Takata K, Taniguchi T (2010) The 6-hydroxydopamine-induced nigrostriatal neurodegeneration produces microglia-like NG2 glial cells in the rat substantia nigra. *Glia* 58:1686–700.

Kösters T, Schäfers KP, Wübbeling F (2011) EMrecon: An expectation maximization based image reconstruction framework for emission tomography data. In *Nuclear Science Symposium and Medical Imaging Conference (NSS/MIC), 2011 IEEE*, pp. 4365–4368.

Kowal SL, Dall TM, Chakrabarti R, Storm MV, Jain A (2013) The current and projected economic burden of Parkinson's disease in the United States. *Mov Disord* 28:311–8.

Lavisse S, Guillermier M, Hérard AS, Petit F, Delahaye M, Van Camp N, Ben Haim L, Lebon V, Remy P, Dollé F, Delzescaux T, Bonvento G, Hantraye P, Escartin C (2012) Reactive astrocytes overexpress TSPO and are detected by TSPO positron emission tomography imaging. *J Neurosci* 32:10809–18.

Levison SW, Goldman JE (1993) Both oligodendrocytes and astrocytes develop from progenitors in the subventricular zone of postnatal rat forebrain. *Neuron* 10:201–12.

Maeda T, Nagata K, Yoshida Y (2008) Exogenous l-DOPA induce no dopamine immuno-reactivity in striatal astroglias and microglias of adult rats with extensive nigro-striatal dopaminergic denervation. *Neurosci. Lett.* 433:255–8.

Maia S, Arlicot N, Vierron E, Bodard S, Vergote J, Guilloteau D, Chalon S (2012)

This article is protected by copyright. All rights reserved.

Longitudinal and parallel monitoring of neuroinflammation and neurodegeneration in a 6-hydroxydopamine rat model of Parkinson's disease. *Synapse* 66:573–83.

McGeer PL, Itagaki S, Boyes BE, McGeer EG (1988) Reactive microglia are positive for HLA-DR in the substantia nigra of Parkinson's and Alzheimer's disease brains. *Neurology* 38:1285–91.

Ming GL, Song H (2011) Adult neurogenesis in the mammalian brain: significant answers and significant questions. *Neuron* 70:687–702.

Nagatsu T, Levitt M, Udenfriend S (1964) Tyrosine hydroxylase. The initial step in norepinephrine biosynthesis. *J Biol Chem* 239:2910–7.

O'Keeffe GC, Barker RA, Caldwell MA (2009) Dopaminergic modulation of neurogenesis in the subventricular zone of the adult brain. *Cell Cycle* 8:2888–94.

Palm T, Hemmer K, Winter J, Fricke IB, Tarbashevich K, Shakib FS, Rudolph IM, Hillje AL, Luca PD, Bahnassawy L, Madel R, Viel T, Siervi AD, Jacobs AH, Diederichs S, Schwamborn JC (2013) A systemic transcriptome analysis reveals the regulation of neural stem cell maintenance by an E2F1-miRNA feedback loop. *Nucleic Acids Res.* 41:3699–712.

Raponi E, Agenes F, Delphin C, Assard N, Baudier J, Legraverend C, Deloulme JC (2007) S100B expression defines a state in which GFAP-expressing cells lose their neural stem cell potential and acquire a more mature developmental stage. *Glia* 55:165–77.

Reumers V, Deroose CM, Krylyshkina O, Nuyts J, Geraerts M, Mortelmans L, Gijsbers R, Van den Haute C, Debyser Z, Baekelandt V (2008) Noninvasive and quantitative monitoring of adult neuronal stem cell migration in mouse brain using bioluminescence imaging. *Stem Cells* 26:2382–90.

Scarf AM, Kassiou M (2011) The translocator protein. *J Nucl Med* 52:677–80.

This article is protected by copyright. All rights reserved.

Accepted Article

Sheng JG, Shirabe S, Nishiyama N, Schwartz JP (1993) Alterations in striatal glial fibrillary acidic protein expression in response to 6-hydroxydopamine-induced denervation. *Exp Brain Res* 95:450–6.

Sierra A, Encinas JM, Deudero JJP, Chancey JH, Enikolopov G, Overstreet-Wadiche LS, Tsirka SE, Maletic-Savatic M (2010) Microglia shape adult hippocampal neurogenesis through apoptosis-coupled phagocytosis. *Cell Stem Cell* 7:483–95.

Swanson LW (2001) Interactive Brain Maps and Atlases In Arbib MA, Grethe JS, editors, *Computing the Brain: A Guide to Neuroinformatics*, pp. 167–77. Academic Press: San Diego.

van den Berge SA, van Strien ME, Korecka JA, Dijkstra AA, Sluijs JA, Kooijman L, Eggers R, Filippis LD, Vescovi AL, Verhaagen J, van de Berg WDJ, Hol EM (2011) The proliferative capacity of the subventricular zone is maintained in the parkinsonian brain. *Brain* 134:3249–63.

Viel T, Monfared P, Schelhaas S, Fricke IB, Kuhlmann MT, Fraefel C, Jacobs AH (2013) Optimizing glioblastoma temozolomide chemotherapy employing lentiviral-based anti-MGMT shRNA technology. *Mol. Ther.* 21:570–9.

Vollmar S, Cizek J, Sué M, Klein J, Jacobs AH, Herholz K (2004) VINCI - "Volume Imaging in Neurological Research, C-Registration and ROIs included" pp. 115–31.

Wachter B, Schürger S, Rolinger J, von Ameln-Mayerhofer A, Berg D, Wagner HJ, Kueppers E (2010) Effect of 6-hydroxydopamine (6-OHDA) on proliferation of glial cells in the rat cortex and striatum: evidence for de-differentiation of resident astrocytes. *Cell Tissue Res* 342:147–60.

Walsh S, Finn DP, Dowd E (2011) Time-course of nigrostriatal neurodegeneration and neuroinflammation in the 6-hydroxydopamine-induced axonal and terminal lesion models of Parkinson's disease in the rat. *Neuroscience* 175:251–61.

This article is protected by copyright. All rights reserved.

Accepted Article

Walton NM, Sutter BM, Laywell ED, Levkoff LH, Kearns SM, Marshall GP, Scheffler B, Steindler DA (2006) Microglia instruct subventricular zone neurogenesis. *Glia* 54:815–25.

Worlitzer MM, Bunk EC, Hemmer K, Schwamborn JC (2012) Anti-inflammatory treatment induced regenerative oligodendrogenesis in parkinsonian mice. *Stem Cell Res Ther* 3:33.

FIGURE LEGENDS

Figure 1: Intranigral 6-OHDA infusion leads to a fast degeneration of the nigrostriatal system. (A) Representative pictures of [^{123}I]Ioflupane-SPECT/T2w MRI in 6-OHDA- and vehicle-injected mice at different time points post injection in axial projections of the striatum. (B) Quantification of specific [^{123}I]Ioflupane uptake in the left striatum. (C) Specific striatal [^{123}I]Ioflupane uptake in the right striatum. (D) Specific [^{123}I]Ioflupane uptake ratio striatum left/right. Significance levels: * P<0.05, ** P<0.01, *** P<0.001, Two Way ANOVA. Error bars: *SD*.

Figure 2: Histological validation of 6-OHDA induced neurodegeneration. Representative Tyrosine hydroxylase (TH) immunostainings in the striatum (A) and the substantia nigra (B) at day 8, 15, and 22 post intranigral vehicle or 6-OHDA injection.

Figure 3: Degeneration of dopaminergic neurons is accompanied by acute microglia activation in the substantia nigra. Representative pictures of coregistered [^{18}F]DPA-714-PET/T2w MRI and [^{18}F]DPA-714-PET alone in 6-OHDA- and vehicle-injected mice at different time points post injection in axial views of the substantia nigra (A) or the striatum (B). The white cross marker shows the position of the substantia nigra (A) or the striatum (B).

This article is protected by copyright. All rights reserved.

Accepted Article

Figure 4: Quantification of [^{18}F]DPA-714 uptake in substantia nigra, injection tract and striatum. (A) Signal to background ratio for the left substantia nigra. (B) Nigral uptake ratio left/right. (C) Signal to background ratio for the injection tract. (D) Mean %ID tracer uptake in the injection tract. (E) Quantification of mean striatal tracer uptake ratio left/right. Significance level: * P<0.05, Mann-Whitney Rank Sum Test. Box plot shows median value and upper/lower quartiles. Whiskers display minimal and maximal values obtained. The dotted lines mark the left /right ratio of 1.0.

Figure 5: Histological markers validate presence of micro- and astrogliosis in the substantia nigra, but lack of substantial microgliosis in the striatum.

(A) Costaining for dopaminergic neurons (TH) and microglia (Iba1) in the ipsilateral SN at 8, 15 and 22 dpi. Arrows show microglia cells displaying an activated phenotype. (B) GFAP/TSPO costaining in the ipsilateral SN at 8, 15 and 22 dpi. (C) Microglia (Iba1) staining in the striatum at 8, 15 and 22 dpi. (D) GFAP staining in the striatum at 8, 15 and 22 dpi. (E) Quantification of Iba^{+} cell ratio left/right in the striatum. Two Way ANOVA. Significance level: $P < 0.05$. Error bars: *SD*. (F) Costaining for GFAP (astrocytes) and TSPO (activated microglia) in the striatum at 15 days post lesion. Scale bars: 100 µm.

Figure 6: BLI of subventricular neurogenesis indicates no detectable alterations following chemical lesion. (A) Representative images of BLI signal post virus injection. (B) Representative images of BLI signal pre- and post vehicle or 6-OHDA infusion. Dotted lines mark the region in between anterior OB and SVZ (injection site). (C) The mean OB/SVZ signal ratio after virus injection increases significantly over time. Significance level: vs. week 2 *$P < 0.05$, **$P < 0.01$, ***$P < 001$; vs. week 3 $^{\#}P < 0.05$, $^{\#\#}P < 0.01$; vs. week 4 $^{\S}P < 0.05$; One Way Repeated Measures ANOVA. (D) Relative change of OB signal post 6-

This article is protected by copyright. All rights reserved.

Accepted Article

OHDA/vehicle infusion (relative to the mean value obtained in the two measurements before lesion). (E) No significant change in the relative OB/SVZ ratio was observed between 6-OHDA and vehicle treated groups (relative to the mean value obtained in the two measurements before lesion). Two Way Repeated Measures ANOVA, $F_{1,42}$ = 0.0962, P = 0.765. Significance level: 0.05. Error bars: *SD*.

Figure 7: Dcx expression pattern in the SVZ is unaltered after neurotoxic lesion.

Staining for neuroblasts (Dcx) after intranigral injection of 6-OHDA or vehicle in C57Bl6 mice. Both contra- and ipsilateral SVZ are displayed. Lesion leads to an unchanged expression of Dcx in the contra- and ipsilateral SVZ in both 6-OHDA and vehicle injected animals. The dotted line defines the border of the lateral ventricle. Str: Striatum, LV: lateral ventricle. Scale bar: 50 µm.

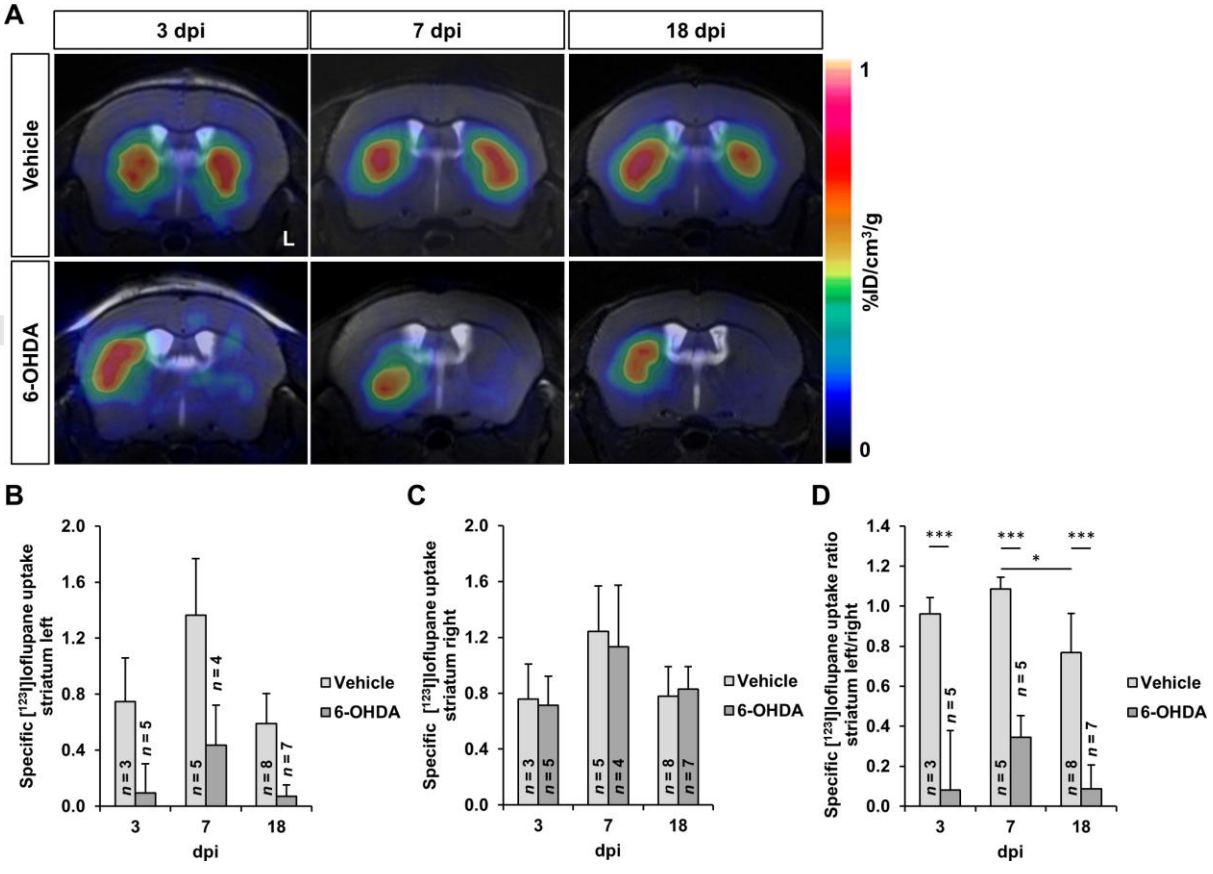

This article is protected by copyright. All rights reserved.

Accepted Article

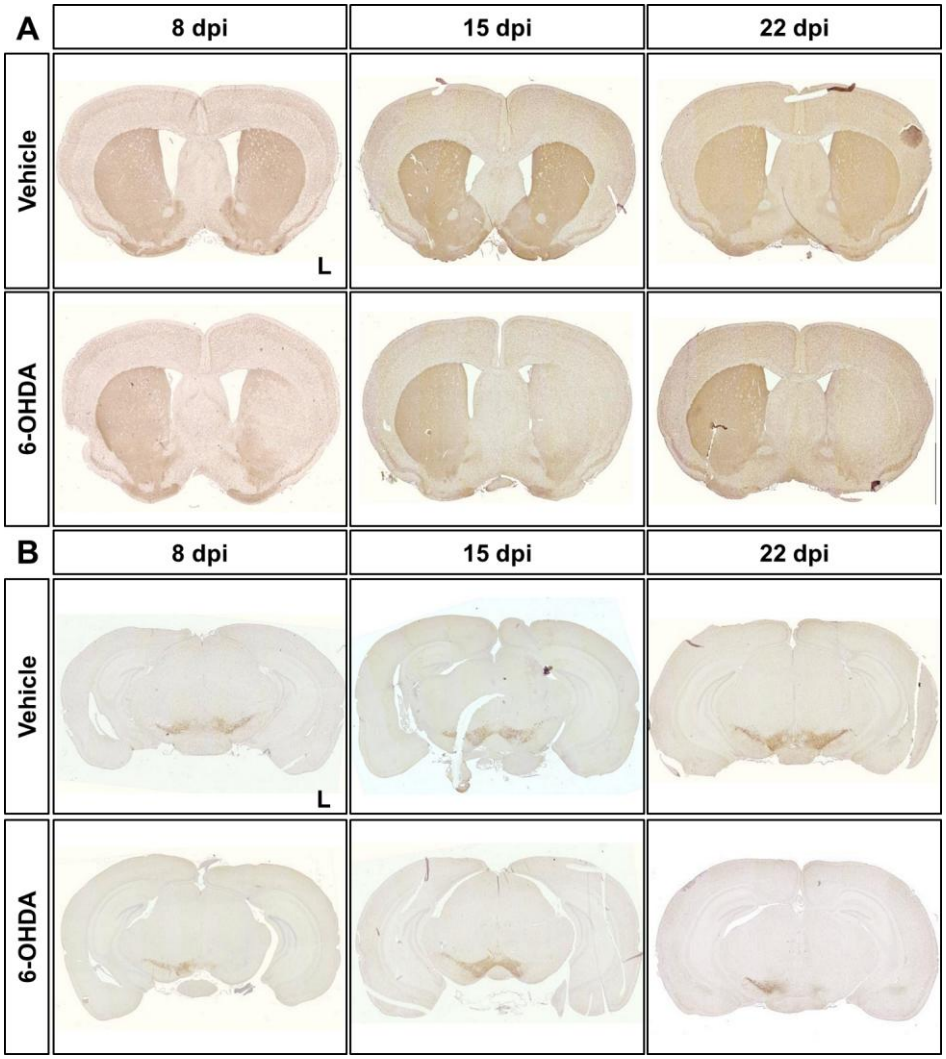

This article is protected by copyright. All rights reserved.

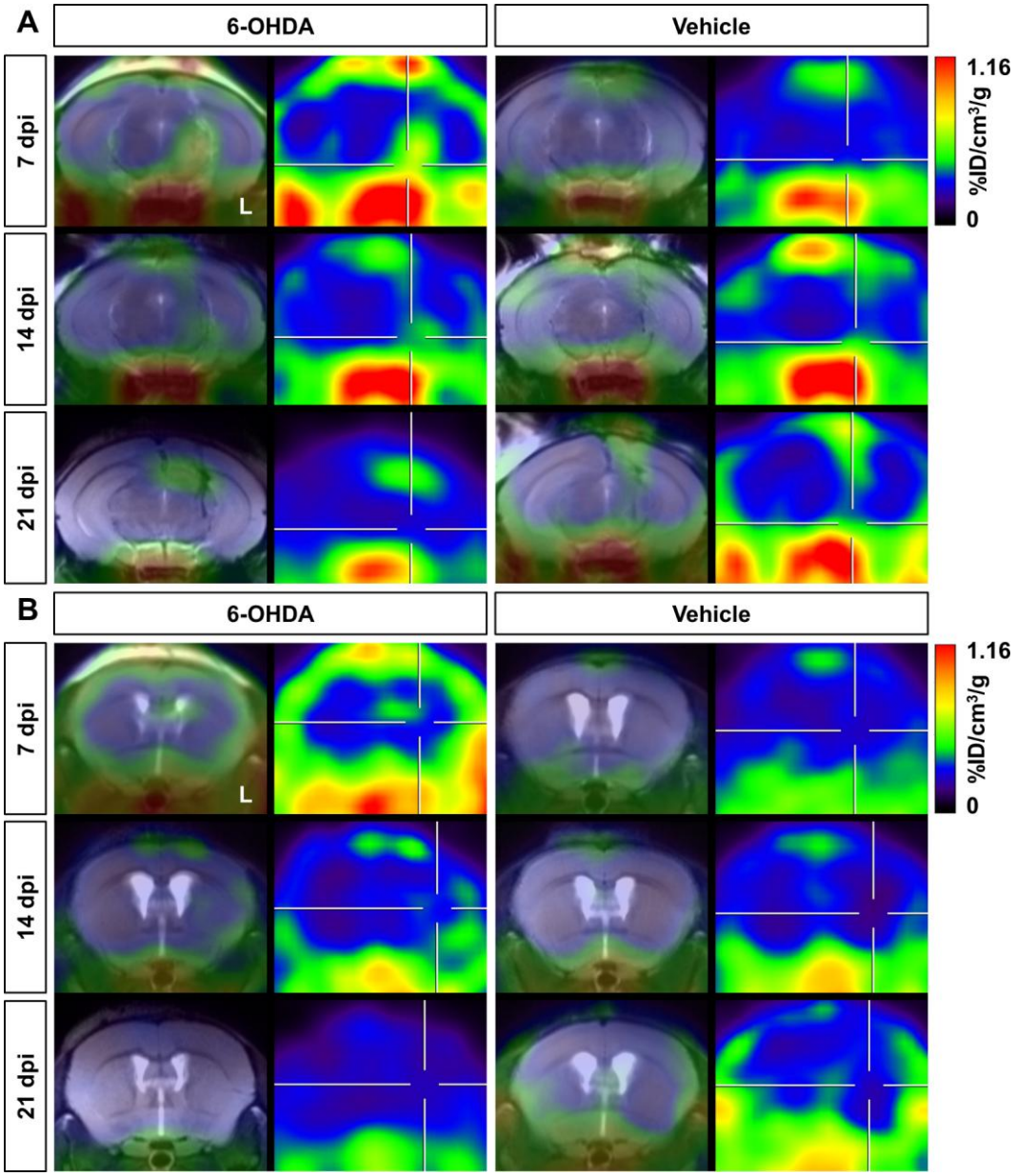

Accepted Article

This article is protected by copyright. All rights reserved.

Accepted Article

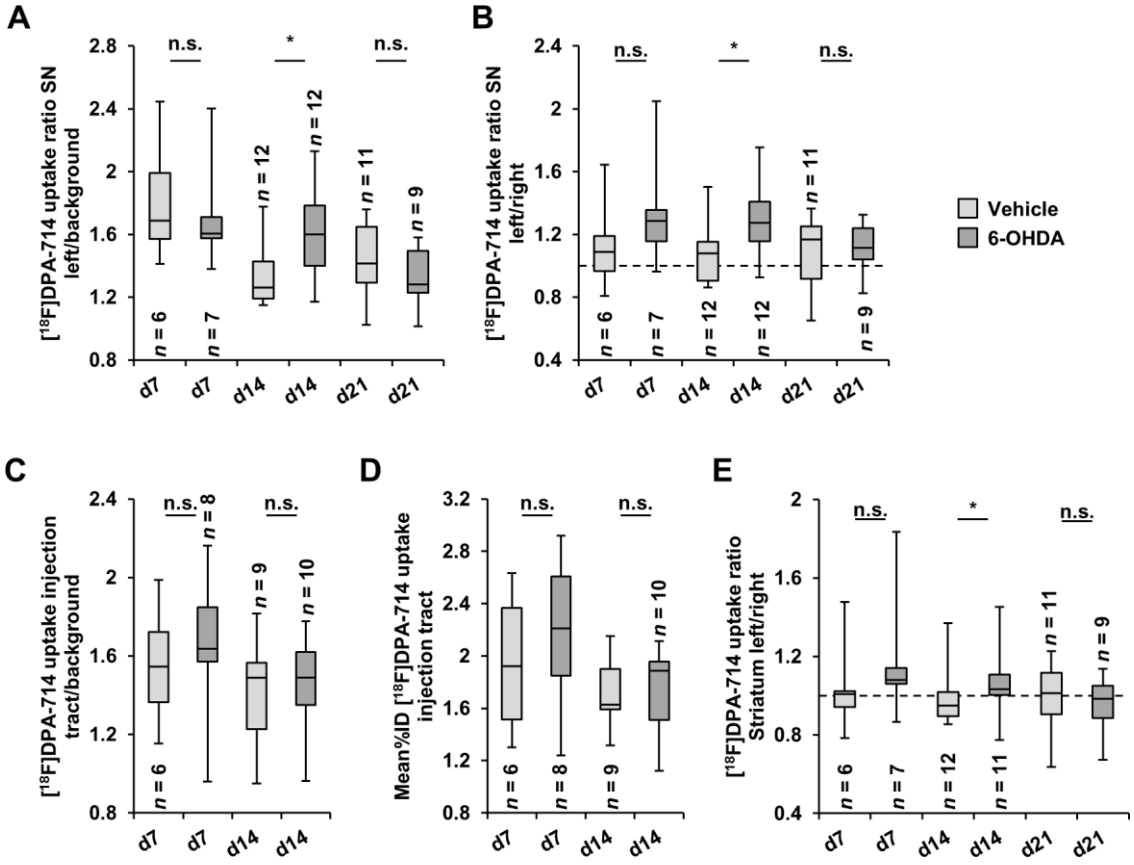

This article is protected by copyright. All rights reserved.

Accepted Article

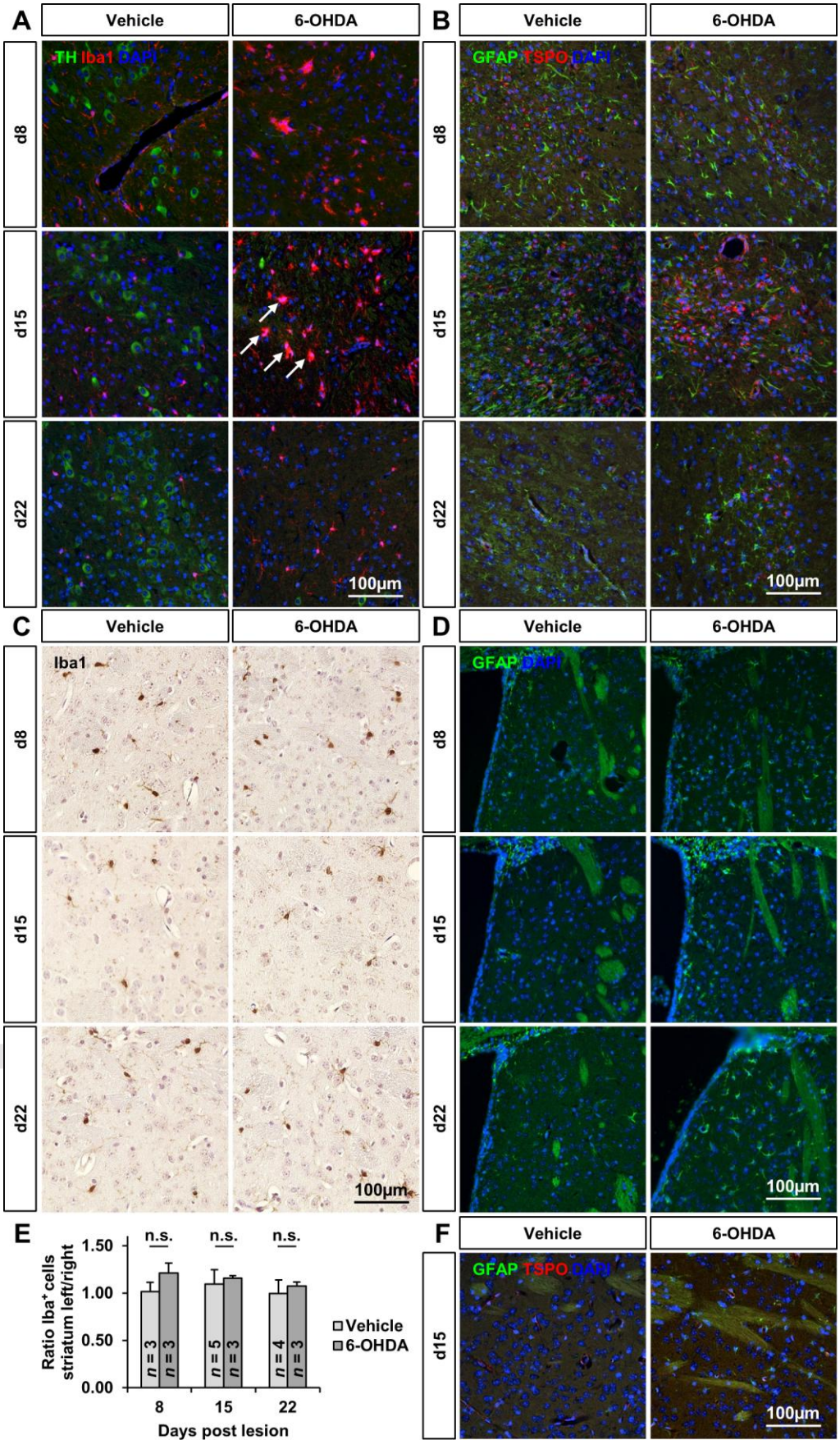

This article is protected by copyright. All rights reserved.

Accepted Article

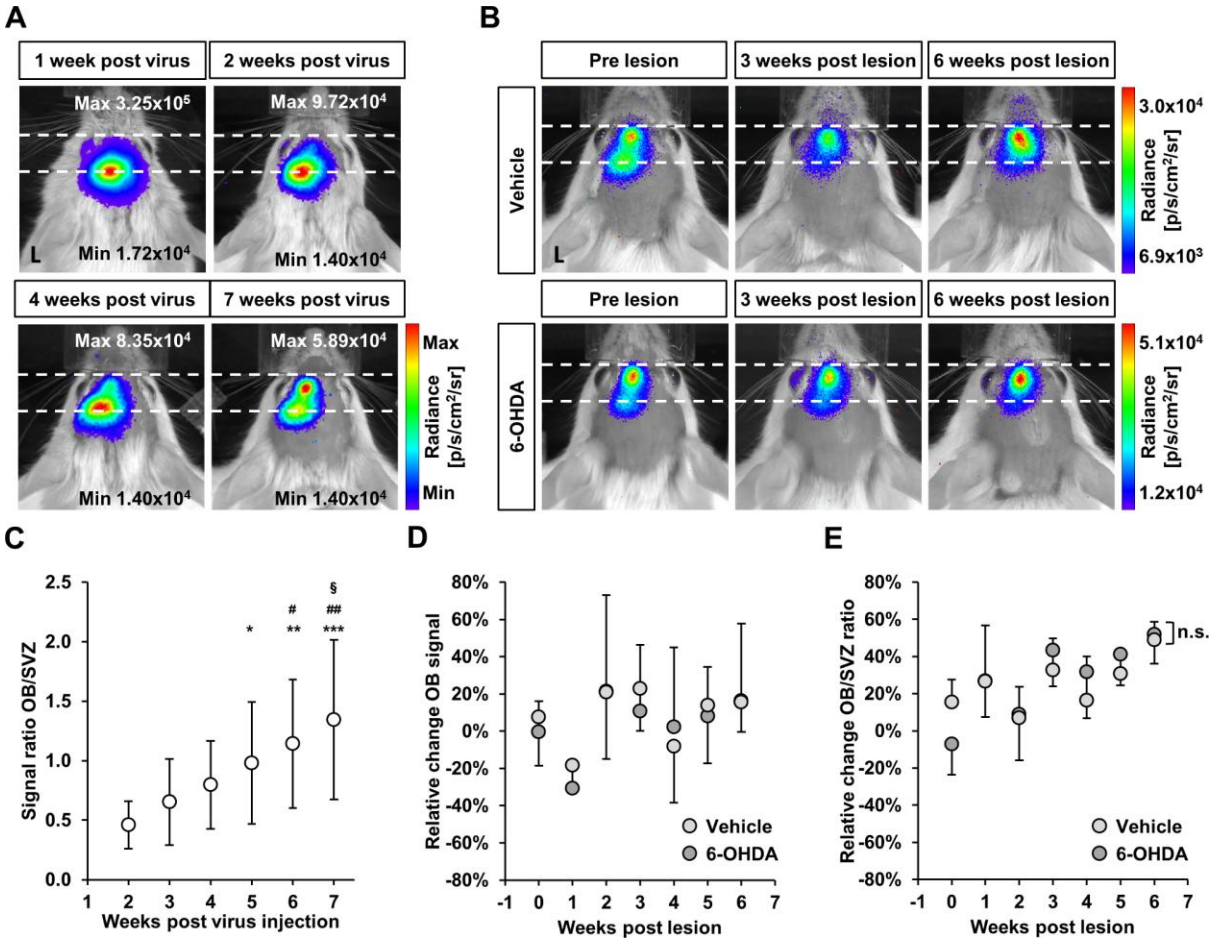

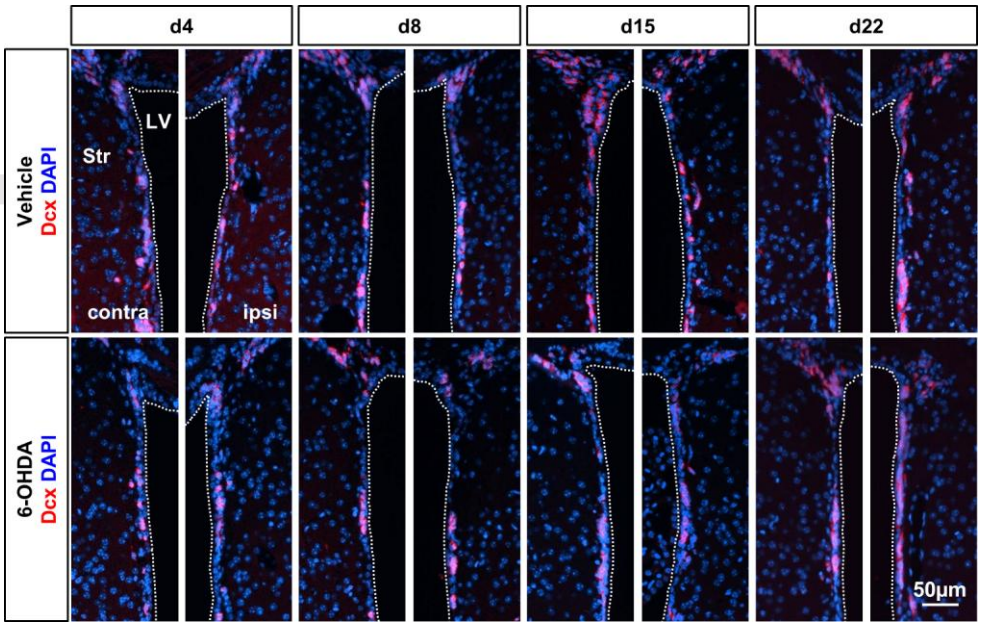

This article is protected by copyright. All rights reserved.